Monte Carlo analysis of drift and diffusion in gaseous Carbon Monoxide

---

The analysis of the electron drift velocity, diffusion and Townsend coefficient in Carbon Monoxide is described and allows an accurate derivation of the various electron scattering processes in the pure gas and its mixtures with Helium and Argon. Some algorithms and functional forms are described as used in Magboltz and Degrade. The derived cross-section set accurately predicts transport properties at the 1% level and is consistent with electron scattering experiments. The sum of the derived cross-sections for singlet excitation at energies above the dissociation energy is in good agreement with the total dissociation cross-section.

This paper outlines the functional forms and procedures that are used here to describe the electron scattering cross-sections from the pure carbon monoxide, CO, and it mixtures with Argon and Helium. We first describe some functional forms and procedures, we then describe the application of them to the experimental transport data in CO and mixtures. The resultant cross-section set is presented in summed graphical form and the calculated transport parameters at room temperature and 77K are shown to be in agreement within the experimental error. Two published data sets (1, 2) for the experimental drift velocity are in disagreement at some electric field values by a combined 3 standard deviation (11%). Using measured electron scattering (13) and theory (16, 17, 18) we reject the measurement (2) and confirm the accuracy of (1).

The first section A) describes some of the functions and algorithms used in the analysis, the second section B) describes the application of the functions to the available transport data.

Section A

Rotation analysis:

The rotational cross-section is described by the functional form given by the born dipole and quadrupole rotators (8). The experimentally measured dipole and quadrupole moments, 0.0432 and 1.46 respectively in atomic units, are used in the calculation of the rotational cross-sections.

The rotations in CO dominate the cross-section at low energy where the dipole cross-section has a maximum below 10 mev and is much larger than the elastic cross-section. The large ratio of inelastic to elastic scattering requires the use of both a momentum transfer and a total cross-section for the inelastic rotational x-section to be used in the calculation of the electron transport in CO. The requirement of using both the momentum transfer and a total cross-section allows the calculated cross-sections to be in agreement with measured (13) elastic and inelastic electron scattering cross-sections and theoretical calculations (16, 17, 18).

The calculation of the momentum transfer x-section from the total cross-section, given by the Born approximation, assumes a point dipole approximation for the angular distribution (32) and has been used previously in magboltz to describe rotational cross-sections in H2O, DME, TMA and alcohols.

The ratio of the momentum transfer to total cross-section is energy dependent and a function of the ratio of the energy loss (transition energy) of the rotation to the incident energy. This simple function allows the efficient calculation of the momentum transfer cross-section from the total x-section. The implementation of the angular scattering is done using the Okhrimovskyy function (33) which is dependent on the above calculated momentum transfer to total cross-section ratio and is of the screened coulomb form. The function is plotted and tabulated on the LXcat website (38).

The experimental (13) measurements and theoretical (16, 17, 18) calculations of the rotation are in approximate agreement except below 10mev. The experimental measurements (13) claim to require a small ~30% reduction in the theoretical born dipole rotations close to the energy threshold of the rotation. However, the accuracy of the experimental data do not exclude the use of the standard Born formula. We have investigated the possible reduction in the rotations close to threshold by using a scaling factor:

Scale Factor = E/(E + Etr)

In the formula the incident electron energy is E and the rotation transition energy is Etr. This functional form is close to that used in the BE formalism (34) which describes the breakdown of the Born cross-section for dipole scattering and is used typically in analysis of scattering from excited states at over 8ev. However it also gives agreement with the reduced cross-section observed in (13). Attempts were made using the scaling factor to fit the drift and diffusion data at 293 and 77K. This scaling factor which would account for the reduction in the experimental electron scattering cross-section was too large to fit the drift and diffusion data and therefore the analysis proceeded with the standard born calculation of the cross-section without a scaling factor.

The quadrupole rotation was also included in the analysis, the quadrupole scattering is much weaker than the dipole scattering and has only ~2 % effect on the calculated transport parameters. The

quadrupole rotation does not require a separate momentum transfer cross-section since it has equal forward and backward scattering and so in this case the quadrupole total rotation cross-section equals the quadrupole momentum transfer cross-section. The quadrupole rotation has a measureable effect only between energies of 0.04 and 0.2ev and was set to zero above 2.0ev where the vibrational energy loss is typically over 100 times larger.

The low energy of the rotational levels lead to a large temperature dependence of the transport parameters. Figure 1 shows the population of the rotational levels at both 77K and 293K.

Vibrational analysis:

The vibrational scattering cross-section is dominated by a large resonance at 1.9ev. The measurements of the first 11 vibrational states by Allan (11) over the energy range of the resonance structure are the most accurate available in the literature. This was confirmed by the very small normalisation of the amplitude of the cross-section required to fit the transport parameters, a normalisation factor of 1.03 was found which is well within the claimed experimental accuracy.

The first vibrational level has a small step at threshold, 0.26573ev, which extends up to the start o**f** the resonance structure at 0.9ev. The measurements of the step structure in electron scattering experiments is difficult due to the small residual energy of the inelastic scattered electron. Accurate measurements of the shape of this step were made by Sohn (14) and were used in the range between threshold and 0.9ev then smoothly joined to Allans cross-section above 0.9ev. The amplitude of this step was taken as a variable in the transport analysis and the result was a reduction of about 30% in the amplitude of the step measured by Sohn. This reduction is consistent the experimental accuracy of 30%.

Excitation analysis:

The excitations in CO are split into singlet and triplet excitations. The singlet excitations are dipole coupled transitions to the ground state and can be accurately calculated using the BE formula (34), which corrects the Born dipole approximation at energies close to threshold.

The born singlet dipole cross-sections are calculated using the measured oscillator strength functions for each level or continuum region. The BE formula and the born dipole are smooth functions and do not include any resonance structures. In applications where there are strong resonance structures which are experimentally measured such as the noble gases it can be used at energies above 3 times the threshold energy of the transition with good accuracy and the resonance structure used closer to threshold. However in most molecular gases this resonance structure is reduced and a good approximation is to use the BE born formula down to threshold. The limiting accuracy in the analysis is not the ignoring of any resonance structure but the lack of good quality triplet scattering data above the first few triplet states.

The experimental dipole oscillator strengths were derived mainly from integrating tables of oscillator strength from (19, 20, 21, 22). The integrations were performed over obvious structures in the oscillator strength that can be assigned to levels below ionisation threshold. Above ionisation threshold the oscillator strength is split into continuum energy loss regions of typically 0.25ev spacing. These continuum integrals represent the neutral dissociation when multiplied by the factor: 1-Qieff (E), where Qieff(E) is the quantum ionisation efficiency (22). The first moment of the continuum integrals above ionisation threshold can also be used to derive the ionisation matrix elements (22) when multiplied by Qieff(E).

The triplet states at and below 12.8ev are taken from experimental measurements (23, 31) without scaling. Above 13ev, where there is no accurate experimental data, the remaining triplet scattering strength is assumed to be in two effective levels at 13.1ev and at 16.8ev.

The amplitude of the 13.1 and 16.8ev effective triplet sums are varied in the analysis to fit the Townsend gain coefficient, this procedure thus allows a minimum of variables to affect the calculation of the Townsend coefficient.

Ionisation analysis:

Experimental measurements of total and dissociative ionisation (26, 29) are used to derive the total ionisation x-section between threshold and 1000ev. The measurements of dissociative ionisation (26, 27, 28) allows the splitting of the total ionisation into dissociative and non-dissociative processes. The further measurement by Liu and Victor (24) allows the splitting of the singly ionised CO+ cross-section into the three allowed CO+ excited states. In total the ionisation can be split into 10 ionisation energy loss channels which sum to the measured total ionisation cross-section.

In the energy range from 1 Kev to 5 Kev the total ionisation is given by the BEB formalism as implemented on the NIST web site(36).

At energies above 5 Kev the total ionisation can be smoothly joined to the functional fully relativistic form (30):

Sigmaion= 1.874*(M2*X1 + C*X2) in units of 10**-20 cm**2

X1= (Beta**-2)*log(beta**2/(1.0-beta**2)) X2= Beta**-2 and Beta=v/c

Where M2 is the ionisation matrix element, 3.26 and C is a constant 38.0.

The value of M2 is obtained from the integral of the first moment of the above ionisation oscillator strength using the quantum ionisation efficiency of Holland (19). The value of M2 and C was experimentally measured by Rieke and Prepejchal (30). However, there are systematic shifts in the data which lead to large correlation between M2 and C in the experiment. The Rieke data were reanalysed using the more accurate M2 value derived here and resulted in the value of C used in this analysis.

In order to extend the partial ionisation x-sections to higher energy it was assumed that at 1 Kev the fractional branching of the 10 ionisation channels were already at their asymptotic fractional values. Given that the total ionisation cross-section is given above 1 Kev by the above formulae then the 10 partial cross-sections can be extended above 1 Kev.

Elastic analysis:

The elastic scattering can be described by either a momentum transfer x-section or a total elastic cross-section with an angular distribution modelled by Okhrimovskyy angular scattering using the shielded coulomb scattering. The fit to the transport data using the elastic momentum transfer cross-section was completed first. Then, using experimentally measured total elastic scattering x-sections the Okhrimovskyy function can be calculated and the predictions of the effect of angular scattering can be obtained in a consistent manner. Measurable effects of angular elastic scattering can only be observed above 200Td where it can cause greater than 1% effects on the transport parameters.

At high electron energies above 5 Kev there are no experimental measurements of the total or momentum transfer elastic cross-section so fully relativistic Hartree-Fock values (35) are used without shadowing correction and smoothly joined to the derived lower energy elastic total and momentum transfer x-sections.

The cross-sections are extended past the minimum ionising range and used in the calculations of range and fano factors in the program degrade (37).

Section B

Analysis of transport data.

The transport data analysis can be split into three energy regions those where the transport data were primarily dependent on the rotational, vibrational or excitation scattering.

At the lowest electric field values below 0.3 Td the rotation determines the drift velocity and diffusion. Between 0.3 and 1.0Td there is a small dependence on the elastic scattering.

At intermediate electric fields between 1.0 and 30 Td the transport parameters are more dependent on the vibrational and elastic cross-sections. In this electric field region there is a much greater transport sensitivity to the vibrational resonance structure in the Argon CO mixture data than in the pure gas. In the argon CO mixture analysis the vibrational scaling correction 1.03 was determined and kept fixed for the analysis of the pure gas data. The analysis of the pure gas transport data then is determined only by varying the elastic scattering cross-section. The He-CO mixture data was used to limit the amplitude of the threshold step in the V1 vibration cross-section since the He-CO mixture data extended to swarm energies that were more sensitive to the vibrational step.

At high electric fields the Townsend coefficient is sensitive to the amplitude of the two summed triplet levels at 13.1 and 16.8ev. The amplitudes of the triplets were varied until good agreement was obtained with the measured Townsend coefficients.

All the above procedures were repeated and in two or three iterations the calculated cross-sections rapidly converged to good fits to the transport parameters in the pure gas and the mixtures.

Results:

Calculated transport parameters:

The derived cross-sections are shown in figure [2]. The rotations are sums of 56 dipole transitions and 54 quadrupole transitions. The vibrations are the sum of 11 levels and the triplet and singlets are the sums of 12 and 70 levels respectively. The ionisation is the sum of 10 dissociative and non-dissociative levels and the very small attachment cross-section is also shown. The sum of the cross-sections is within 1% of the accurately measured total cross-section (23).

Figure 3 shows the calculated and measured values of the drift velocity in Ar-CO and He-CO mixtures the average deviation between calculation and experiment is about 0.4% in the Ar-CO and 0.5% in He-CO mixtures. The experimental values (3) are quoted as having 3% maximum errors.

The drift and diffusion data in pure gas was measured in a few papers (1,2,7,10), unfortunately there is some disagreement between the two most accurate measurements at the level of 3 times the combined experimental errors in some regions of low electric field. Attempts to fit the data of Petrovic (2) gave an elastic x-section which had a large dip in the elastic scattering at 0.1ev, the dip has not been observed in the elastic scattering experiments or predicted by theory (16, 17, 18). The data of Petrovic (2) was rejected in the regions where it disagreed with Nakamura (1) and as can be seen in Figure 4 the drift velocity of Nakamura is fit within the 2% experimental error. The room temperature measurements of the transverse and longitudinal diffusion are also calculated to be within the larger experimental errors of 5% and shown in Figure 5.

Measurements of drift velocity and diffusion at 77 Kelvin, although not as accurate as at room temperature, are shown in Figure 6 and Figure 7 respectively. The experimental measurements of the transverse diffusion show an offset from the theoretically correct constant value at low electric field but are otherwise in reasonable agreement with the calculation within experimental error. The drift velocity at 77K shows a peak at 0.38 Td with a very shallow dip followed by a rise. This is first observation of negative differential conductivity in the literature although it was not recognised at the time. The peak is driven by the shape of the rotational and elastic cross-sections.

The total dissociation cross-section has been measured by Cosby (15) and is shown in Figure 8 along with the cross-section sum of the singlets with energies above the dissociation threshold. The results show good consistency in shape and amplitude and limit the triplet dissociation to less than 10% of the singlet dissociation.

The calculation of the Fano Factor and W, the energy required to produce an ion pair are important for the use of the cross-sections in radiation modelling and astrophysics (24). The asymptotic W value calculated with Degrade using the derived cross-sections is 32.5ev, in good agreement with the measurement of 32.2ev.

In conclusion a complete set of Carbon Monoxide electron scattering cross-sections is presented which accurately predict the electron transport parameters over the temperature range from 77 to 300K. There are some obvious limitations to this analysis caused by the disagreements between experimental drift velocity measurements and also the lack of good quality transverse diffusion measurements at 77K.

Show alpha/N, eta/N vs E/N.

Figure 1. Final set of cross sections

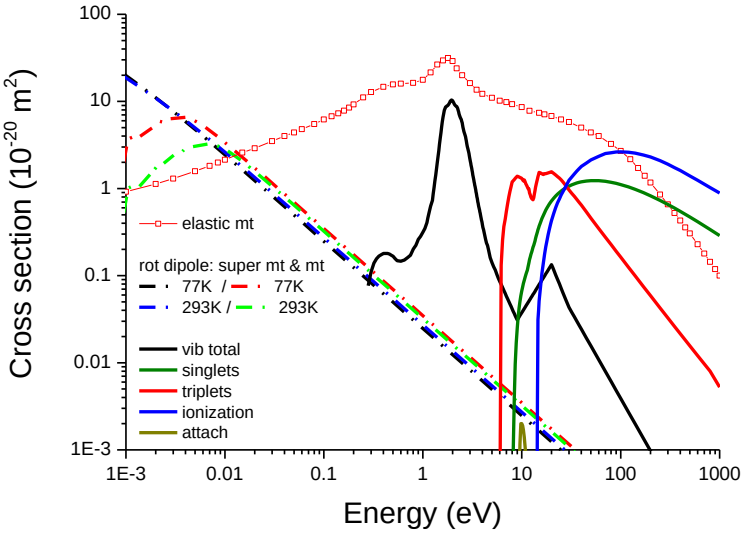

Fig 2a drift velocity, expt+calc in Ar/CO mixtures

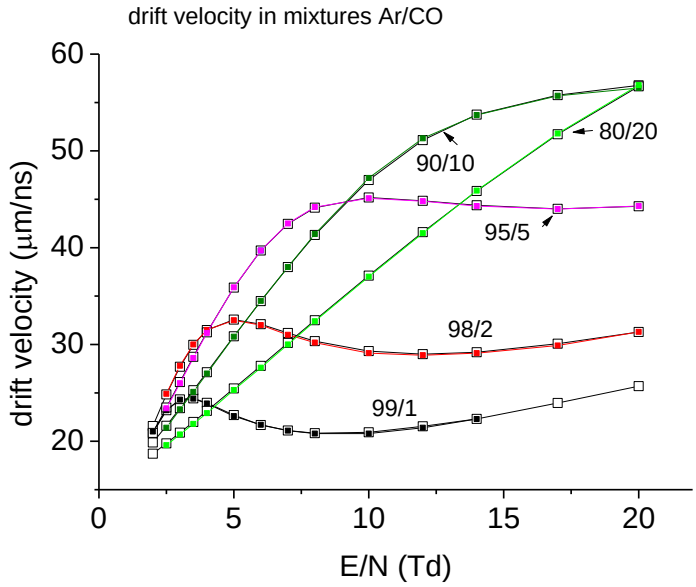

Fig 2b drift velocity, expt+calc in He/CO mixtures

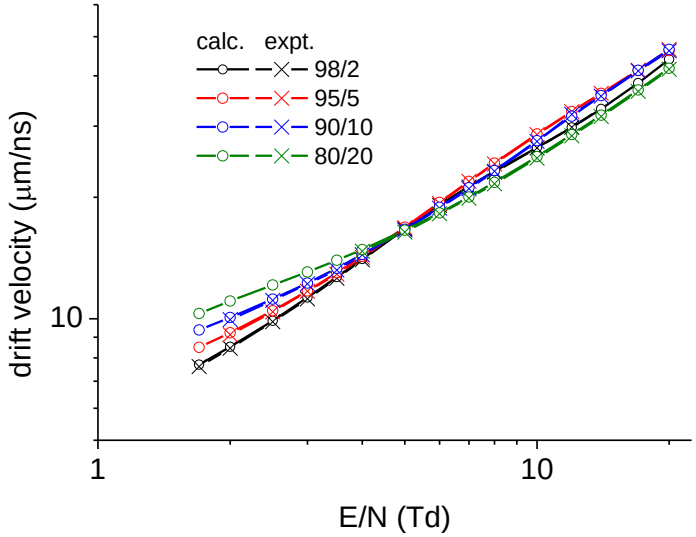

Or is it better with another scale in E/N?

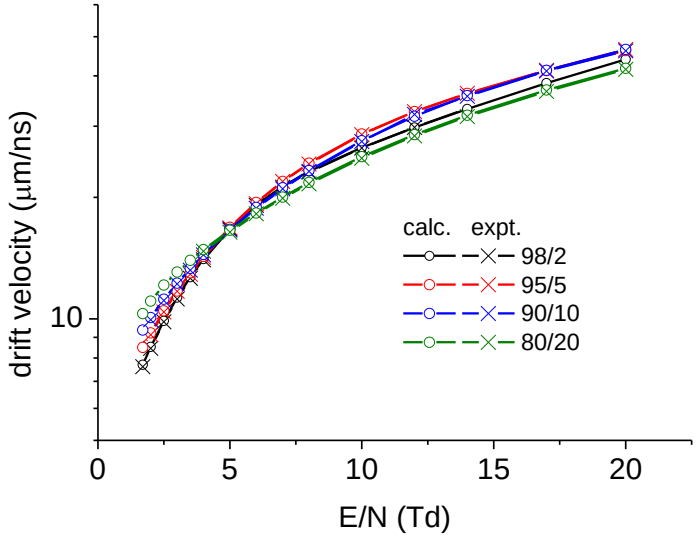

Fig 3. Drift velocity, expt + calc, pure gas

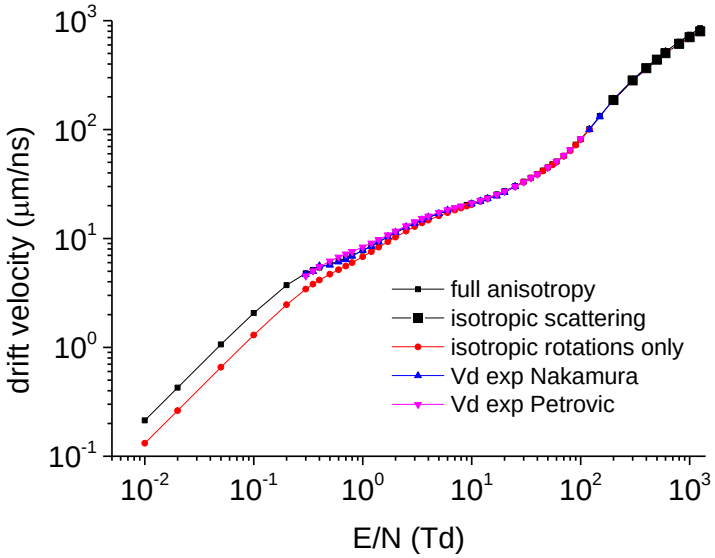

Fig. 4. DT/mu and DL/mu

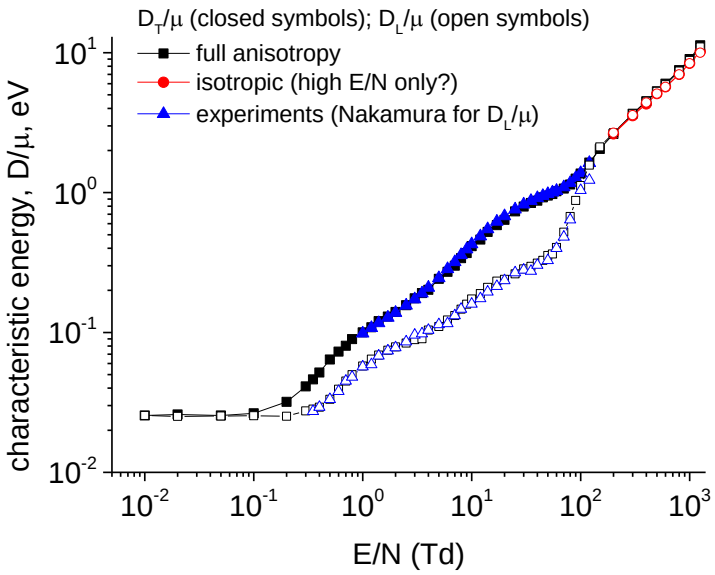

Fig. 5. Drift velocity in CO at 77K, expt + calc

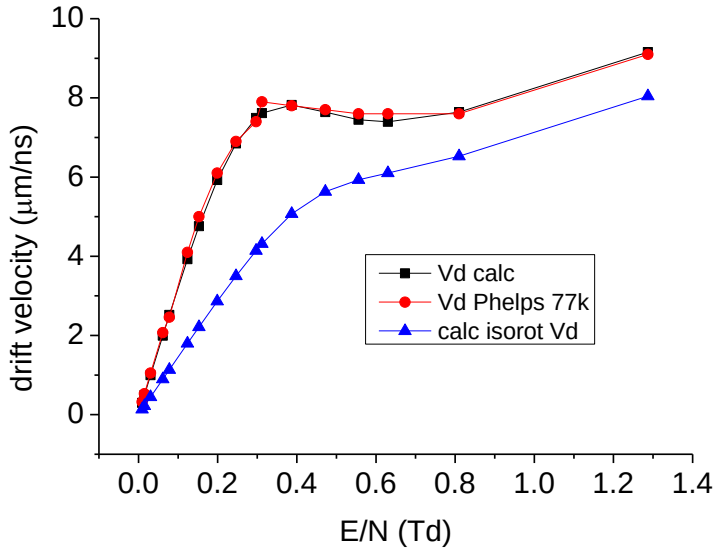

Fig. 6. DT/mu (expt + calc) and DL/mu (calc) at 77K in pour CO

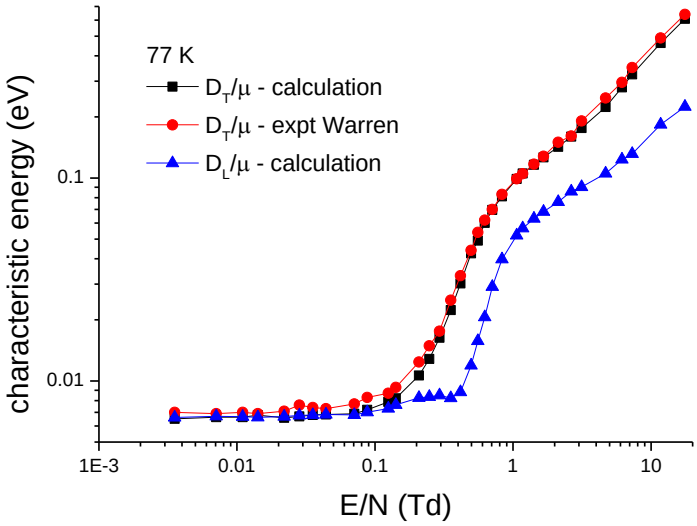

Fig. 7. Dissociation cross section determined from sum of singlet excitation (?) compared to Cosby expt.

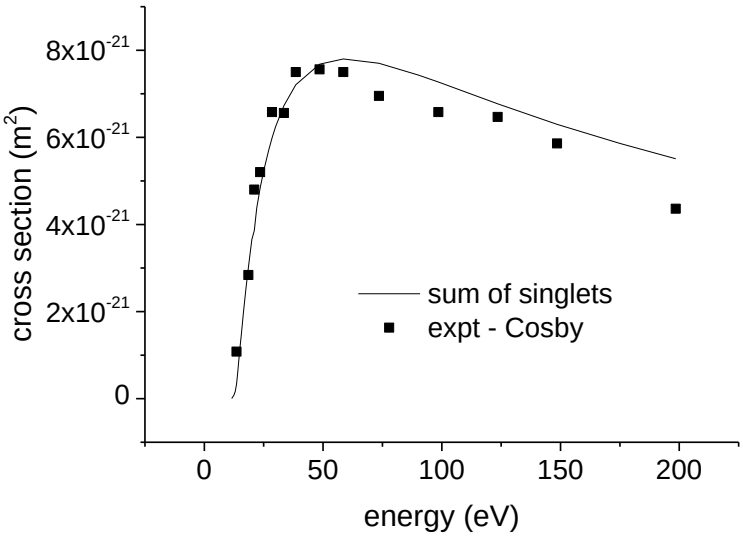

Alpha and eta – Townsend coefficients for number changing processes

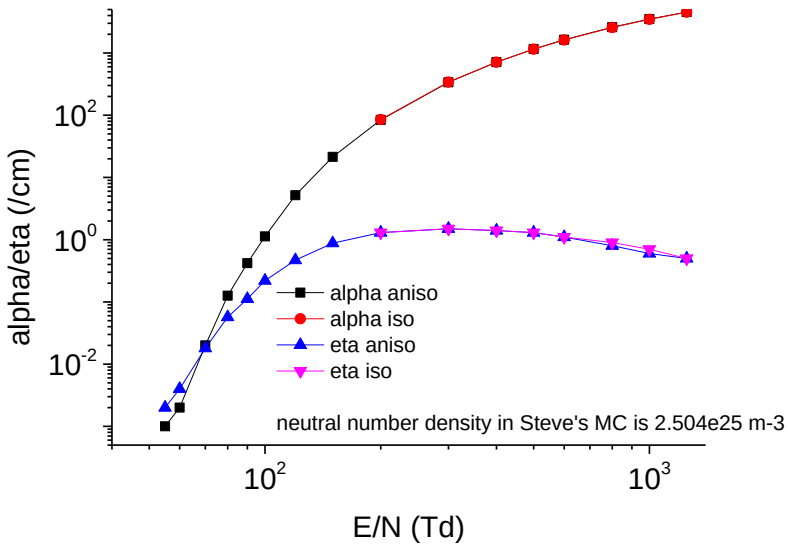

For info: relative population in rotational levels

In MAGBOLTZ subroutine gas23

```
B0=2.3836D-4
    DO 4 K=1,28 (K is rotational level)
    AK=DFLOAT(K)
  4 PJ(K)=(2.0*AK+1.0)*DEXP(-AK*(AK+1.0)*B0/AKT)

Where AKT=(ABZERO+TEMPC)*BOLTZ
 BOLTZ=8.6173324D-5
```

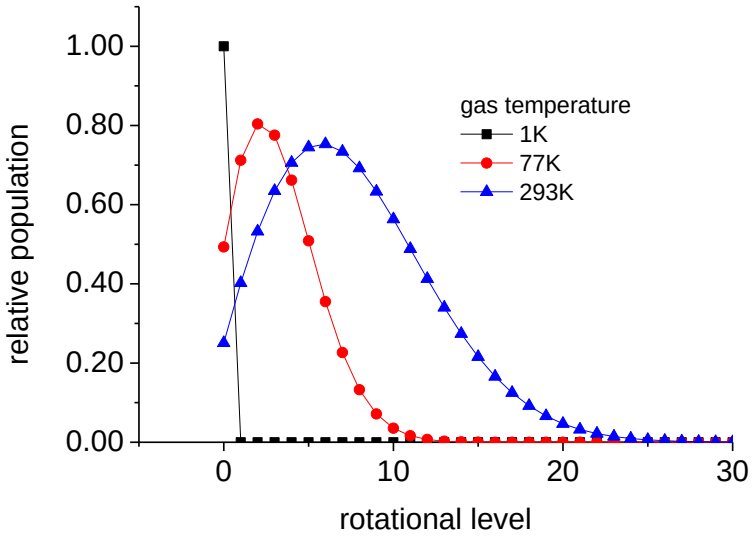

References:

1 Y.Nakamura J.Phys.D. 20 (1987)933

2 Z.L.Petrovic and R.W.Crompton Aust.J.Phys. 42(1989)609

3 G.N.Haddad and H.B.Milloy Aust.J.Phys. 36(1983)473

4 J.L.Pack and A.V.Phelps Phys.Rev. 121(1961)798

5 G.Ramanan and G.R.Freeman J.Chem.Phys. 95(1991)4195

6 H.T.Saelee and J.Lucas J.Phys.D. 10(1977)343

7 J.Dutton J.Phys.Chem.Ref.Data 4(1975)577

8 R.D.Hake and A.V.Phelps Phys.Rev. 158(1967)70

9 C.S.Lakshminarasimha,J.Lucas and N.Kontoleon J.Phys.D. 7(1974)2545

10 R.W.Warren and J.H.Parker Phys.Rev. 128(1962)2661

11 M.Allan Phys.Rev.A. 81(2010)042706

12 J.Gibson,L.A.Morgan,R.J.Gulley,M.J.Brunger,
C.T.Bundschu and S.J.Buckman J.Phys.B. 29(1996)3197

13 J.Randall,R.J.Gulley,S.Lunt,J-P.Ziesel and D.Field J.Phys.B. 29(1996)2049

14 W.Sohn,K-H.Kochem,K.Jung,H.Ehrhardt and E.S.Chang J.Phys.B. 18(1985)2049

15 P.C.Cosby J.Chem.Phys. 98(1993)7804

16 N.Chandra Phys.Rev.A 12(1975)2342

17 N.Chandra Phys.Rev.A 16(1977)80

18 A.Jain and D.W.Norcross Phys.Rev.A 45(1992)1644

19 W.F.Chan,G.Cooper and C.E.Brion Chem.Phys. 170(1993)123

20 D.M.P.Holland and D.A.Shaw J.Phys.B 53(2020)144004

21 Sakamoto,Berkowitz et al NIFS-DATA-109 (2010)

22 J.Berkowitz Atomic and Molecular Photoasborption Academic Press (2002)

23 Y.Itikawa J.Phys.Chem.Ref.Data 44(2015)013105

24 W.Liu and G.A.Victor Astro.Phys.J. 435(1994)909

25 J.M.Ajello J.Chem.Phys. 55(1971)3158

26 M.A.Mangan,B.G.Lindsay and R.F.Stebbings J.Phys.B 33(2000)3225

27 C.Tian and C.R.Vidal Phys.Rev. 59(1999)1955

28 C.Tian and C.R.Vidal J.Phys.B 31(1998)895

29 D.Rapp and P.Englander-Golden Phys.Rev. 43(1965)1464

30 F.F.Rieke and W.Prepejchal Phys.Rev.A 6(1972)1507

31 M.Zawadzki,M.A.Khakoo et al J.PhysB. 53(2020)165201

32 K.F.Ness and R.E.Robson Phys.Rev.A 38(1988)1446

33 A.Okhrimovskky,A.Bogaerts and R.Gijbels Phys.Rev.E 65(2002)037402

34 Y-K.Kim J.Chem.Phys 126(2007)064305

35 R.Mayol and F.Salvat At.Nucl.Data Tables 65(1997)55

36 NIST https://physics.nist.gov/PhysRefData/Ionisation/intro.html

37 Magboltz https://magboltz.web.cern.ch/magboltz

Degrade https://degrad.web.cern.ch/degrad

38 Lxcat https://nl.lxcat.net/home/